Comparative Analysis of Two Mathematical Models of Single Diode Photovoltaic Cells for Extracting PV Parameters Using Levenberg – Marquardt Algorithm

Youssef Chahet[1*], *Abdelmalek* Mimouni[2], *Abdellatif* Bouaichi[3], *Mohamed* El Amraoui[1], *Aumeur* El Amrani[2], and *Lahcen* Bejjit[2]

[1]LASMAR, Faculty of Sciences, Moulay Ismail University of Meknes, Morocco
[2]MIN research Group, LASMAR, ESTM, Moulay Ismail University of Meknes, Morocco
[3]SMARTi Laboratory, EMSI Rabat, Morocco

Abstract. In this present study, two mathematical models derived from the single-diode model of photovoltaic (PV) cells and modules are evaluated. Moreover, the two mathematical approaches are investigated for the reduced single-diode model and the reduced single-diode combined to Lambert W-function model. The Levenberg-Marquardt optimization algorithm is chosen due to its effectiveness in addressing the complex optimization problems encountered in PV cells modeling. The comparative analysis evaluated the accuracy and computational efficiency of the both models for three PV datasets obtained from the literature. The results demonstrated that the combination of the reduced single-diode with Lambert W-function model achieves a minimum RMSE value of 3.1627×10^{-4}, compared to the reduced single-diode model one of 3.2066×10^{-4}.

1 Introduction

Solar energy is the most suitable and promising alternative to generate electricity among all renewable energy sources, especially in locations with high solar radiation [1,2]. Furthermore, photovoltaic (PV) cells and modules convert solar radiation directly into electrical energy using the photovoltaic effect, and their development enhance the energy conversion and reduce the overall costs [3–5]. Therefore, appropriate PV cell models are crucial in solar power generation to estimate the I-V curve, which is measured using two methods: online and offline methods. The online methods necessitate large resources and long-term computations. On the other hand, offline methods predict the I-V curve using dynamic models at various environmental conditions [5].

Various factors influence the PV cell as well as module performance, such as temperature, irradiance, and aging. Therefore, the modification of intrinsic parameters of solar cells, which directly impact module efficiency. Hence, an appropriate model of PV cells and modules is required to accurately estimate such parameters.

* Corresponding author: youssef.chahet@edu.umi.ac.ma.

In the literature, single-diode and double-diode are the most common models used as equivalent circuits to represent the behaviour of physical solar cells and modules [6]. The single diode is accurate and simple to implement, while the double diode, especially in low solar irradiance, is more precise but needs longer computational time [7]. The PV parameters estimation techniques have been classified into two main categories: analytical and numerical methods [5]. Analytical methods attempt to find a mathematical relationship between the key points provided by the manufacturer's datasheet to obtain the model parameters. Moreover, the mathematical equation that describes the I-V characteristic of the PV cells is a non-linear problem, which requires the introduction of assumptions or approximations in the derivative process in order to be solved. While analytical methods are relatively fast and straightforward, the lack of provided points of I–V characteristic limits their accuracy.

Numerical approaches are curve fitting algorithms that use optimization algorithms to find the error between theoretical an experimental I-V characteristics. These algorithms can be organized in two categories: iterative and meta-heuristic optimization methods. Iterative methods tend to trap in local minimum if the initial parameters are far from the optimum. Hence, the introduction of meta-heuristic algorithms, which gain popularity in the recent years for handling non-linear equations and global search. One such category is that of evolutionary algorithms (EAs), which include: particle swarm optimization (PSO) [8], artificial bee swarm optimization (ABSO) [9], bird mating optimizer (BMO) [10], genetic algorithm (GA) [11], simulated annealing (SA) [12], and pattern search (PS) [13]. Although the iterative optimization methods may be susceptible to being trapped in local minimum, this can be avoided with the proper choice of initial values for input parameters. This approach solves the issue of local minima and enhances the overall performance of the optimization process.

The purpose of this work is to extract PV device parameters using two mathematical models. The first is a reduced single diode model, and the second is the same model with the addition of the Lambert W-function to ascertain whether it can enhance the overall performance.

This paper is organized as follows: the second section presents the two mathematical models; the third section introduces the Levenberg-Marquardt algorithm, initial parameter value determination, and statistical criteria for evaluating the algorithm; the fourth section presents the results of evaluating both mathematical models with three available PV data sets from the literature: R.T.C. France solar cell and two PV modules, Photowatt PWP201, and Leybold (STE 4/100) PV solar modules; and finally, section five summarizes the work.

2 Photovoltaic model

2.1 Single diode model of solar cell

Fig. 1. illustrates the single-diode equivalent circuit of a PV cell, which contains photogenerated current (I_{ph}), diode current (I_d), R_s and R_{sh} are the series and shunt resistances. Kirchhoff's law is used to calculate the output current as [14]:

$$I = I_{ph} - I_d - I_{sh} \tag{1}$$

Where the term I refers to the output current and I_{sh} to shunt resistor current. In addition, I_d represents the Shockley equation as follows:

$$I_d = I_0 \left[\exp\left(\frac{V + R_s.I}{N_s.V_t.n}\right) - 1 \right] \tag{2}$$

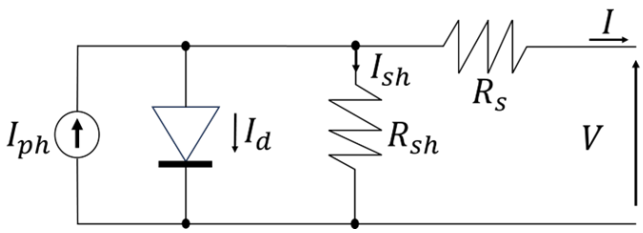

Fig. 1. Equivalent circuit of the single diode model for a PV cell.

With, I_0 represents the reverse saturation or leakage current of the diode, V denotes the output voltage, N_s refers the number of connected cells in series, n is the ideality factor, and V_t is the thermal voltage:

$$V_t = \frac{k.T}{q} \tag{3}$$

Where T refers to the cell temperature (K), k denotes the Boltzmann constant ($1.3806503 \times 10^{-23}$ J/K), and q is the electron charge ($1.60217646 \times 10^{-19}$ C).
The shunt resistor current I_{sh} is calculated using the following equation:

$$I_{sh} = \frac{V + R_s.I}{R_{sh}} \tag{4}$$

By combining all the equations from (1) to (4), the resulting equation for the output current is given as follows:

$$I = I_{ph} - I_0\left[\exp\left(\frac{V + R_s.I}{N_s.V_t.n}\right) - 1\right] - \frac{V + R_s.I}{R_{sh}} \tag{5}$$

In this model there are five unknown parameters that need to be identified from the single-diode model, which are (I_{ph}, I_0, R_s, R_{sh}, n). Through mathematical conduct, we reduced the number of parameters to three (R_s, R_{sh}, n) [15]. At open circuit voltage (V_{oc}) and short circuit current (I_{sc}), equation (5) becomes as:

$$\begin{cases} V = V_{oc} \\ I = 0 \end{cases} \Rightarrow 0 = I_{pv} - I_0.\left(\exp\left(\frac{V_{oc}}{N_s.V_t.n}\right) - 1\right) - \frac{V_{oc}}{R_{sh}} \tag{6}$$

$$\begin{cases} V = 0 \\ I = I_{sc} \end{cases} \Rightarrow I_{sc} = I_{ph} - I_0.\left(\exp\left(\frac{R_s.I_{sc}}{N_s.V_t.n}\right) - 1\right) - I_{sc}.\frac{R_s}{R_{sh}} \tag{7}$$

By using equations (6) and (7) for I_{ph} and I_0, we can find the following formulas:

$$I_0 = \frac{\left[I_{sc}\left(1 + \frac{R_s}{R_{sh}}\right) - \frac{V_{oc}}{R_{sh}}\right].\exp\left(-\frac{V_{oc}}{N_s.V_t.n}\right)}{1 - \exp\left(\frac{R_s.I_{sc} - V_{oc}}{N_s.V_t.n}\right)} \tag{8}$$

$$I_0 + I_{ph} = \frac{I_{sc}\left(1 + \frac{R_s}{R_{sh}}\right) - \frac{V_{oc}}{R_{sh}}}{1 - \exp\left(\frac{R_s.I_{sc} - V_{oc}}{N_s.V_t.n}\right)} + \frac{V_{oc}}{R_{sh}} \tag{9}$$

Substituting equations (8) and (9) into equation (5), the terms I_{ph} and I_0 can be replaced, and consequently the equation (5) can be written as follows:

$$I = \frac{V_{oc} - V - I.R_s}{R_{sh}} - \frac{\left[I_{sc}\left(1 + \frac{R_s}{R_{sh}}\right) - \frac{V_{oc}}{R_{sh}} \right].\left(\exp\left(-\frac{V_{oc} - V - I.R_s}{N_s.V_t.n} \right) - 1 \right)}{1 - \exp\left(\frac{R_s.I_{sc} - V_{oc}}{N_s.V_t.n} \right)} \tag{10}$$

2.2 Lambert W-function

The Lambert W-function is employed to ascertain whether it can enhance the performance of the reduced single-diode model. A detailed manipulation of the aforementioned formula for the calculation of I using the Lambert W-function is provided below:
First, rearrange equation (5) by multiplying R_{sh} as depicted in the equation (11) below:

$$I = \frac{\left(I_{ph} + I_0\right).R_{sh} - I_0.R_{sh}.\exp\left(\frac{V + R_s.I}{N_s.V_t.n} \right) - V}{R_s + R_{sh}} \tag{11}$$

Then, multiplying by R_s to both sides as:

$$I.R_s = \frac{R_s}{R_s + R_{sh}}\left(\left(I_{ph} + I_0\right).R_{sh} - I_0.R_{sh}.\exp\left(\frac{V + R_s.I}{N_s.V_t.n} \right) - V \right) \tag{12}$$

Adding V to both sides:

$$I.R_s + V = \frac{R_s}{R_s + R_{sh}}\left(\left(I_{ph} + I_0\right).R_{sh} - I_0.R_{sh}.\exp\left(\frac{V + R_s.I}{N_s.V_t.n} \right) - V.\frac{R_s}{R_{sh}} \right) \tag{13}$$

Divide by $N_s.V_t.n$ and rearrange:

$$\begin{aligned} &\frac{I.R_s + V}{N_s.V_t.n} + \frac{I_0.R_s.R_{sh}}{N_s.V_t.n.\left(R_s + R_{sh}\right)}.\exp\left(\frac{V + R_s.I}{N_s.V_t.n} \right) \\ &= \frac{R_s}{N_s.V_t.n.\left(R_s + R_{sh}\right)}\left(\left(I_{ph} + I_0\right).R_{sh} - V.\frac{R_s}{R_{sh}} \right) \end{aligned} \tag{14}$$

Exponential for both sides:

$$\begin{aligned} &\exp\left(\frac{I.R_s + V}{N_s.V_t.n} \right).\exp\left[\frac{I_0.R_s.R_{sh}}{N_s.V_t.n.\left(R_s + R_{sh}\right)}.\exp\left(\frac{V + R_s.I}{N_s.V_t.n} \right) \right] \\ &= \exp\left[\frac{R_s}{N_s.V_t.n.\left(R_s + R_{sh}\right)}\left(\left(I_{ph} + I_0\right).R_{sh} - V.\frac{R_s}{R_{sh}} \right) \right] \end{aligned} \tag{15}$$

Multiply both sides by $\frac{I_0.R_s.R_{sh}}{N_s.V_t.n.(R_s + R_{sh})}$

$$\begin{aligned} &\frac{I_0.R_s.R_{sh}}{N_s.V_t.n.\left(R_s + R_{sh}\right)}.\exp\left(\frac{I.R_s + V}{N_s.V_t.n} \right).\exp\left[\frac{I_0.R_s.R_{sh}}{N_s.V_t.n.\left(R_s + R_{sh}\right)}.\exp\left(\frac{V + R_s.I}{N_s.V_t.n} \right) \right] \\ &= \frac{I_0.R_s.R_{sh}}{N_s.V_t.n.\left(R_s + R_{sh}\right)}\exp\left[\frac{R_s}{N_s.V_t.n.\left(R_s + R_{sh}\right)}\left(\left(I_{ph} + I_0\right).R_{sh} - V.\frac{R_s}{R_{sh}} \right) \right] \end{aligned} \tag{16}$$

Now, Lambert W-function (W_0) can be applied. Once again, rearrange both sides of the equation of I which is depicted in equation (17) as follows:

$$-I.\left(R_s+R_{sh}\right)+\left(I_{ph}+I_0\right).R_{sh}-V$$
$$=\frac{N_s.V_t.n.\left(R_s+R_{sh}\right)}{R_s}.W_0\left(\frac{I_0.R_s.R_{sh}}{N_s.V_t.n.\left(R_s+R_{sh}\right)}\exp\left(\frac{R_{sh}.\left(I_{ph}.R_s+I_0.R_s+V\right)}{N_s.V_t.n.\left(R_s+R_{sh}\right)}\right)\right) \quad (17)$$

Then,

$$I=\frac{N_s.V_t.n}{R_s}.W_0\left(\frac{I_0.R_s.R_{sh}}{N_s.V_t.n.(R_s+R_{sh})}\exp\left(\frac{R_{sh}.\left(R_s.\left(I_{ph}+I_0\right)+V\right)}{N_s.V_t.n.(R_s+R_{sh})}\right)\right)-\frac{V-\left(I_{ph}+I_0\right).R_{sh}}{R_s+R_{sh}} \quad (18)$$

By replacing $(I_{ph}+I_0)$ and I_0 in the equation (18) above, the Lambert W-function mathematical model obtained as follow:

$$I=X_1-X_2.W_0\left\{X_3.\exp\left(X_4\right)\right\} \quad (19)$$

With:

$$X_1=\frac{\frac{I_{sc}\left(1+\frac{R_s}{R_{sh}}\right)-\frac{V_{oc}}{R_{sh}}}{1-\exp\left(\frac{R_s.I_{sc}-V_{oc}}{N_s.V_t.n}\right)}+\frac{V_{oc}}{R_{sh}}-\frac{V}{R_{sh}}}{1+\frac{R_s}{R_{sh}}} \quad (20)$$

$$X_2=\frac{N_s.V_t.n}{R_s} \quad (21)$$

$$X_3=\frac{\frac{R_s}{N_s.V_t.n}.\exp\left(-\frac{V_{oc}}{N_s.V_t.n}\right)}{1+\frac{R_s}{R_{sh}}}.\frac{\left[I_{sc}\left(1+\frac{R_s}{R_{sh}}\right)-\frac{V_{oc}}{R_{sh}}\right].\exp\left(-\frac{V_{oc}}{N_s.V_t.n}\right)}{1-\exp\left(\frac{R_s.I_{sc}-V_{oc}}{N_s.V_t.n}\right)} \quad (22)$$

And

$$X_4=\frac{\frac{R_s}{N_s.V_t.n}}{1+\frac{R_s}{R_{sh}}}\left[\frac{I_{sc}\left(1+\frac{R_s}{R_{sh}}\right)-\frac{V_{oc}}{R_{sh}}}{1-\exp\left(\frac{R_s.I_{sc}-V_{oc}}{N_s.V_t.n}\right)}+\frac{V_{oc}}{R_{sh}}-\frac{V}{R_{sh}}\right] \quad (23)$$

3 Optimization Algorithm

3.1 Levenberg-Marquardt Algorithm

The Levenberg-Marquardt (LM) algorithm was developed to solve non-linear least squares problems. Its equation is presented as follows [15]:

$$(\underline{J}^T\underline{J}+\lambda.diag[\underline{J}^T\underline{J}]).\delta\underline{\beta}=\underline{J}^T[\underline{I}-\underline{f}(\underline{V})] \quad (24)$$

where $\underline{f}(\underline{V})=I_k^{th}$ and $\underline{I}=\{I_k^{\exp}\}_{k=1..N}$, and $\underline{J}$ is the Jacobian of f whose k_{th} row equal $\underline{J}_k$:

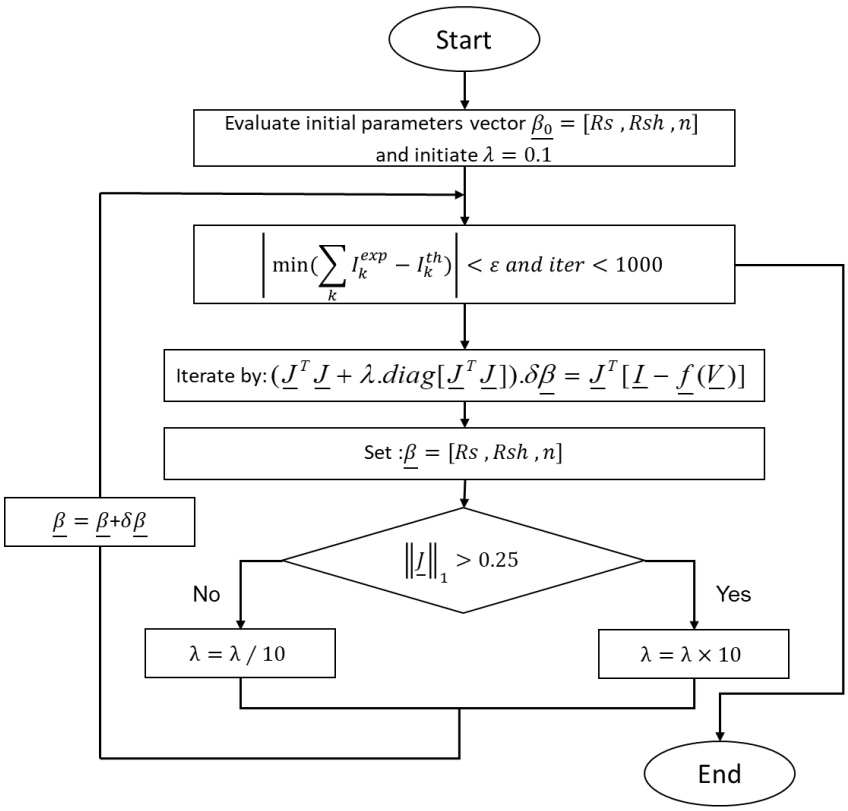

Fig. 2. Flowchart of the Levenberg-Marquardt algorithm.

$$\underline{J} = \begin{pmatrix} \frac{\partial f(V_1)}{\partial R_s} & \frac{\partial f(V_1)}{\partial R_{sh}} & \frac{\partial f(V_1)}{\partial n} \\ \frac{\partial f(V_2)}{\partial R_s} & \frac{\partial f(V_2)}{\partial R_{sh}} & \frac{\partial f(V_2)}{\partial n} \\ \vdots & \vdots & \vdots \\ \frac{\partial f(V_N)}{\partial R_s} & \frac{\partial f(V_N)}{\partial R_{sh}} & \frac{\partial f(V_N)}{\partial n} \end{pmatrix} \tag{25}$$

The damping factor, $\lambda > 0$, and the vector, $\underline{\boldsymbol{\beta}} = [R_s, R_{sh}, n]$, are the two key variables. As illustrated in Figure 2, these two parameters are adjustable in each iteration.

3.2 Initial values

The LM algorithm, similar to other gradient-descent based methods, requires an initial value for (R_s, R_{sh}, n), to overcome the issue of local minimum trapping. There are numerous methods for calculating the initial values of R_s and R_{sh}, such as reported in [14]. However, to extract the initial values, we utilized the experimental I-V curve, applying linear regression near the short-circuit and open-circuit points. The intercepts of two polynomial equations with the I-axis and V-axis, as illustrated in Figure 3, were employed to determine the slopes, denoted as, a_1 and a_2 in the following equations:

$$I_1 = a_1 V + b_1 \tag{26}$$

$$I_2 = a_2 V + b_2 \tag{27}$$

The detailed calculation of R_s, R_{sh}, and n value are described in [16] as follows:

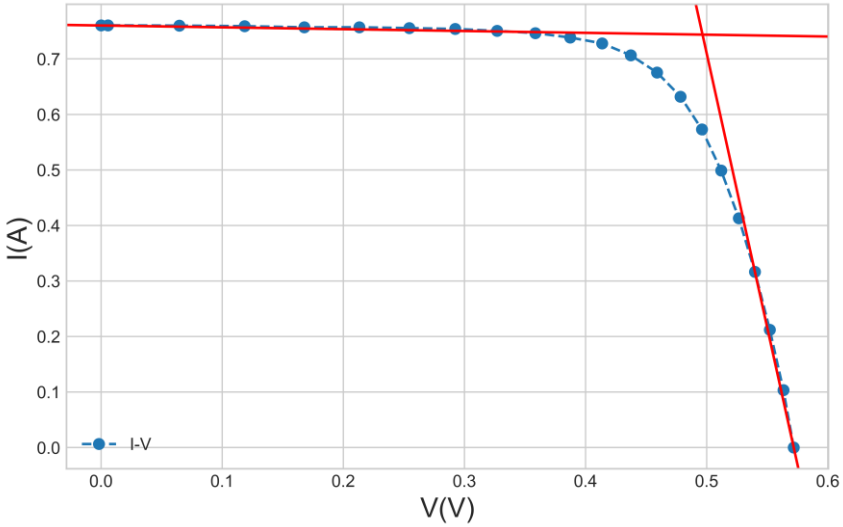

Fig. 3. The interception of the two polynomials with I-axis and V-axis.

$$\begin{cases} R_{sh}^{(0)} = \left| -\dfrac{1}{a_1} \right| \\ R_s^{(0)} = \left| \left(-\dfrac{1}{R_{sh}^{(0)}.a_2} - 1 \right) \dfrac{N_s.V_t.n^{(0)}}{I_0^{(0)}} . \exp\left(-\dfrac{V_{oc}}{N_s.V_t.n^{(0)}} \right) \right| \\ n^{(0)} = 1.5 \end{cases} \tag{28}$$

3.3 Statistical criteria

The root mean squared error (RMSE) is a statistical metric that measures the deviation between the experimental and theoretical I–V curve of a sample of N measured points, which can be expressed as follows:

$$RMSE = \sqrt{\frac{1}{N} \sum_{k=1}^{N} \left[I_k^{\exp} - I_k^{th} \right]^2} \tag{29}$$

Where I_k^{exp} and I_k^{th} are the kth measured and theoretical current, respectively.

4 Results and discussion

The performance of LM algorithm was evaluated using, R.T.C. France solar cell and two PV modules, which are: Photowatt PWP201 solar module, and Leybold solar module (STE 4/100). The I-V characteristic of the R.T.C. France solar cell was taken under 1000W/m^2 and at an operating cell temperature of 33ºC [17]. The results of the application of LM algorithm

for both reduced single-diode model and W-function model fit well with the experimental curve as shown in Figure 4 for R.T.C. France solar cell. Although there is a difference between the extracted values as presented in Table 1. As illustrated in Figure 5, the RMSE values of 2.39×10^{-3} and 2.48×10^{-3} were noticed for the reduced single diode model and W-function model, respectively. It should be noticed that not all points from the I-V curve were considered in this analysis; only those between (0, I_{sc}) and (V_{oc}, 0) were included. The complete set of data points can be found in the appendix. Consequently, when our results are compared to those of literature, our algorithm exhibited a slight deficiency in terms of RMSE. However, the algorithm demonstrates a high level of convergence efficiency, requiring only 9 iterations to reach a solution for LM-RSD and 11 iterations for LM-Wf.

Photowatt PWP201 module is investigated, which contains 36 polycrystalline silicon cells in series, and operated at $45\ °C$ and $1000\ W/m^2$ [17]. Moreover, also only the points between (0, I_{sc}) and (V_{oc}, 0) were considered. In contrast to the R.T.C. France solar cell, the algorithm demonstrated satisfactory performance, especially for LM-RSD, which is within the range of other algorithms reported in the literature, as illustrated in Table 2. The RMSE values for the LM-RSD and LM-Wf algorithms are 2.461×10^{-3} and 4.481×10^{-3}, respectively. Additionally, the measured and theoretical data exhibited a high degree of correlation as shown in Figure 6, also as described in Figure 7. We noticed that the number of iterations was 8 for LM-RSD and 11 iterations for LM-Wf.

The last Leybold solar module (STE 4/100) is studied, it consist of 4 polycrystalline series connected cells, which measured data was conducted at module temperature of $22\ ºC$ and under indoor light of $900\ W/m^2$ [6], and all the data points was fed to the algorithm. Interestingly, for this module I-V data both our algorithm outperformed that in [6] as presented in Table 3., with a minimum value of RMSE for LM-Wf of 3.1627×10^{-4}, which indicate that after incorporating all points from the I-V characteristic, our algorithm not only demonstrated excellent performance but also exhibited rapid convergence, as illustrated in Figures 8 and 9.

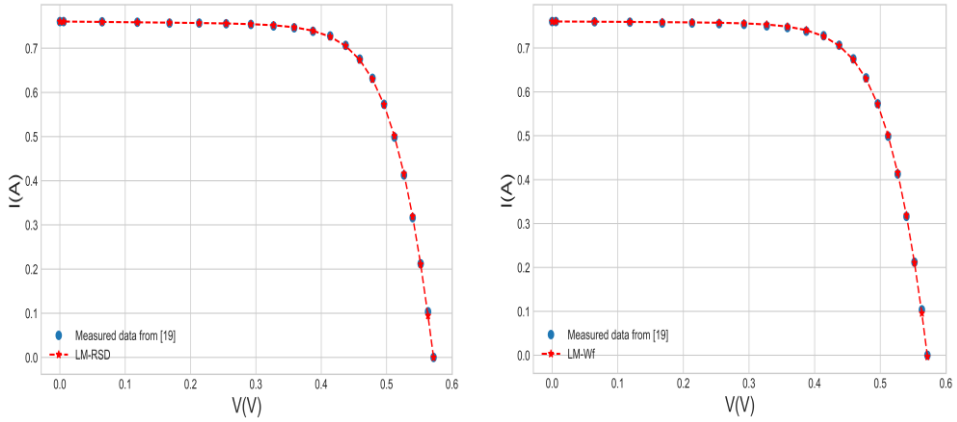

a) LM-RSD b) LM-Wf

Fig. 4. Measured and estimated (I-V) characteristics for R.T.C. France solar cell using LM-RSD and LM-Wf algorithms.

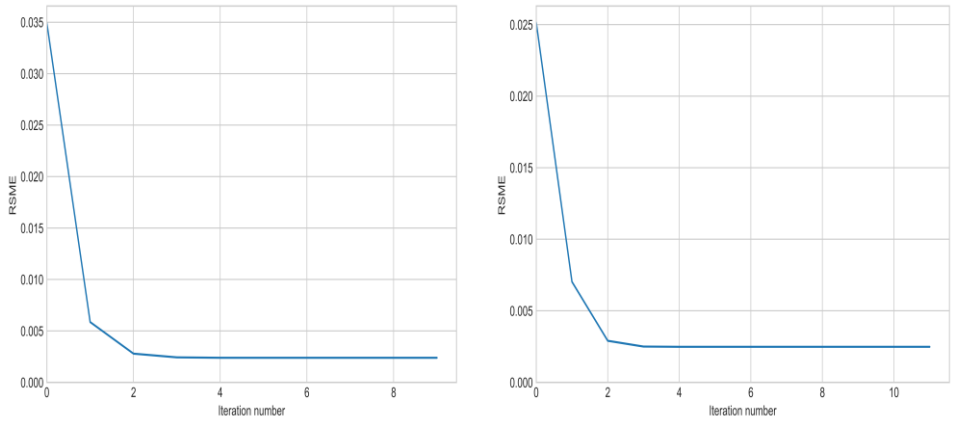

a) Convergence graphs for LM-RSD b) Convergence graphs for LM-Wf

Fig. 5. Convergence graphs of the for R.T.C. France solar cell.

Table 1. Comparison results for R.T.C France solar cell.

Algorithm	R_s **(Ω)**	R_{sh} **(Ω)**	n	**RMSE**
BA [6]	0.0367	52.4722	1.4732	7.7896×10^{-4}
PGJAYA [18]	0.0364	53.7185	1.4812	9.8602×10^{-4}
ILCOA [19]	0.0364	53.7187	1.4811	9.8602×10^{-4}
LM-RSD (This work)	0.0282	66.16	1.585	2.390×10^{-3}
LM-Wf (This work)	0.0252	114.936	1.640	2.484×10^{-3}

Table 2. Comparison results for Photowatt PWP201 module.

Algorithm	R_s **(Ω)**	R_{sh} **(Ω)**	n	**RMSE**
BA [6]	1.218	761.490	1.335	2.125×10^{-3}
PGJAYA [18]	1.201	981.854	1.351	2.425×10^{-3}
HFAPS [20]	1.201	984.281	1.351	2.425×10^{-3}
LM-RSD (This work)	1.247	688.757	1.313	2.461×10^{-3}
LM-Wf (This work)	1.030	1811.309	1.463	4.481×10^{-3}

Table 3. Comparison results for Leybold module (STE 4/100).

Algorithm	R_s **(Ω)**	R_{sh} **(Ω)**	n	**RMSE**
BA [6]	2.5567	2184.82	1.0304	3.3392×10^{-4}
LM-RSD (This work)	0.2493	2652.87	1.3819	3.2066×10^{-4}
LM-Wf (This work)	0.4106	2566.22	1.3482	3.1627×10^{-4}

The performance of both algorithms, LM-RSD and LM-Wf, for the R.T.C. France solar cell and the Photowatt PWP201 module, was found to be inferior compared to their performance with the Leybold module (STE 4/100). This discrepancy was attributed to whether all data points were consistently fed into both algorithms, as previously discussed. Furthermore, both algorithms demonstrated optimal performance with the Leybold module (STE 4/100), particularly in terms of convergence speed and RMSE value. Table 4 illustrates the mean computational time of the algorithms for the 3 PV devices. It should be noticed that the algorithms were coded and executed in Spyder, an integrated development environment. The computational time for each algorithm was determined by a built-in time module in Python. The Spyder software was run on a Dell Latitude E5450 with 8 GB RAM and an Intel Core i5-5300U CPU, 2.3 GHz processor.

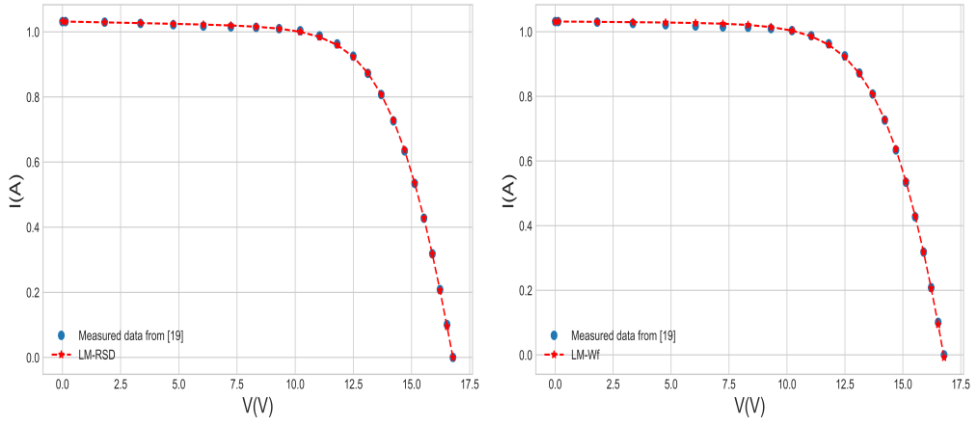

a) LM-RSD b) LM-Wf

Fig. 6. Measured and estimated (I-V) characteristics for Photowatt PWP201 using LM-RSD and LM-Wf algorithms.

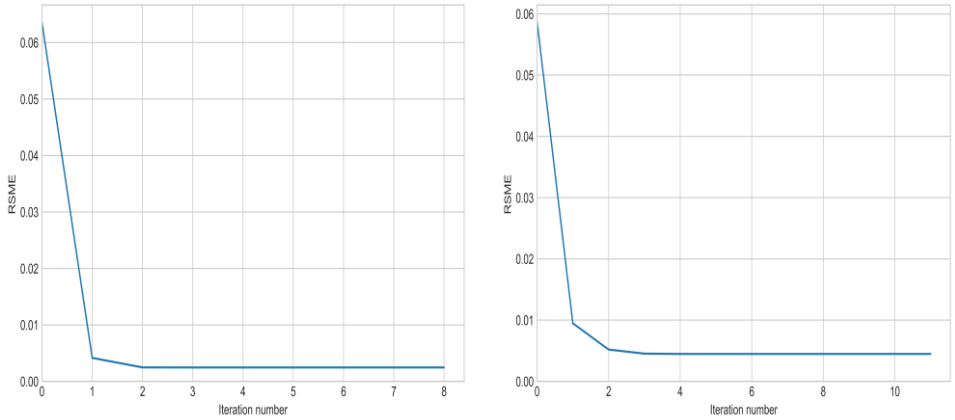

a) Convergence graphs for LM-RSD b) Convergence graphs for LM-Wf

Fig. 7. Convergence graphs of Photowatt PWP201 module.

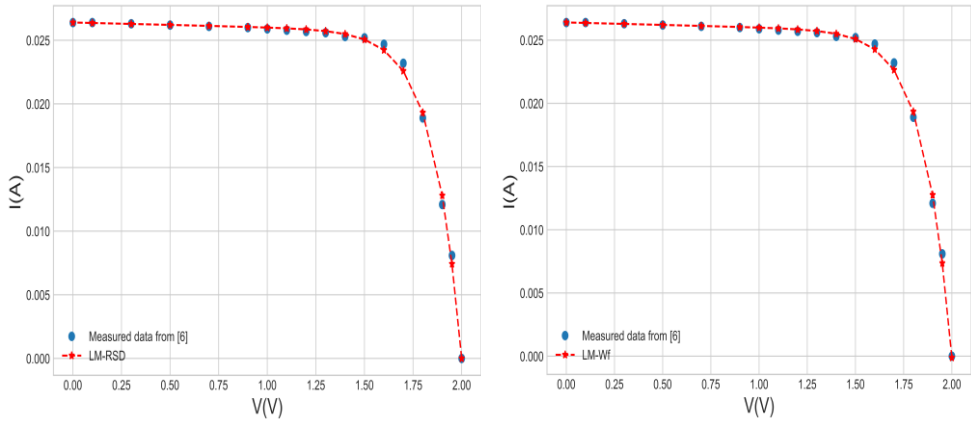

c) LM-RSD d) LM-Wf

Fig. 8. Measured and estimated (I-V) characteristics for Leybold solar module (STE 4/100) using LM-RSD and LM-Wf algorithms.

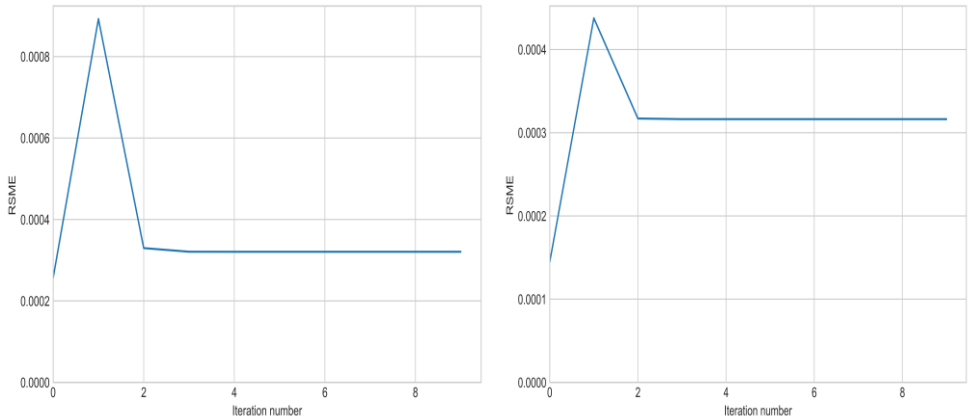

c) Convergence graphs for LM-RSD d) Convergence graphs for LM-Wf

Fig. 9. Convergence graphs of Leybold solar module (STE 4/100).

Table 4. The computational time (s) of R.T.C. France solar cell, Photowatt PWP201, and Leybold module (STE 4/100).

Algorithm	R.T.C. France solar cell	Photowatt PWP201	Leybold module (STE 4/100)
LM-RSD (This work)	38.401	29.372	25.991
LM-Wf (This work)	145.520	151.660	93.922

5 Conclusion

This study presents the results of implementing the Levenberg-Marquardt algorithm to extract the parameters of three photovoltaic devices: the R.T.C. France solar cell, the

Photowatt PWP201 module, and the Leybold module (STE 4/100), using the reduced single diode model and W-function method. The validity of both algorithms is verified using the experimental data from the aforementioned devices. Moreover, the performance of these algorithms is compared to other algorithms in the literature. According to the results, the proposed algorithms yield optimal outcomes when the data points of I-V characteristic are situated within the range of (0, I_{sc}) and (V_{oc}, 0), and have a good combination between convergence speed, accuracy, and computational time.

Appendix

The measured I-V characteristics of the three PV devices [6,19] used in this work.

R.T.C. France solar cell		Photowatt PWP201 module		Leybold solar module (STE 4/100)	
V(V)	I(A)	V(V)	I(A)	V(V)	I(A)
-0.2057	0.764	-1.9426	1.0345	0	0.0264
-0.1291	0.762	0.1248	1.0315	0.1	0.0264
-0.0588	0.7605	1.8093	1.03	0.3	0.0263
0.0057	0.7605	3.3511	1.026	0.5	0.0262
0.0646	0.76	4.7622	1.022	0.7	0.0261
0.1185	0.759	6.0538	1.018	0.9	0.026
0.1678	0.757	7.2364	1.0155	1	0.0259
0.2132	0.757	8.3189	1.014	1.1	0.0258
0.2545	0.7555	9.3097	1.01	1.2	0.0257
0.2924	0.754	10.2163	1.0035	1.3	0.0256
0.3269	0.7505	11.0449	0.988	1.4	0.0253
0.3585	0.7465	11.8018	0.963	1.5	0.0252
0.3873	0.7385	12.4929	0.9255	1.6	0.0247
0.4137	0.728	13.1231	0.8725	1.7	0.0232
0.4373	0.7065	13.6983	0.8075	1.8	0.0189
0.459	0.6755	14.2221	0.7265	1.9	0.0121
0.4784	0.632	14.6995	0.6345	1.95	0.0081
0.496	0.573	15.1346	0.5345	2	0
0.5119	0.499	15.5311	0.4275		
0.5265	0.413	15.8929	0.3185		
0.5398	0.3165	16.2229	0.2085		
0.5521	0.212	16.5241	0.101		
0.5633	0.1035	16.7987	-0.008		
0.5736	-0.01	17.0499	-0.111		
0.5833	-0.123	17.2793	-0.209		
0.59	-0.21	17.4885	-0.303		

References

1. A. Luque and S. Hegedus, Handbook of Photovoltaic Science and Engineering, 1st ed. (Wiley, 2010).
2. A. Bouraiou, M. Hamouda, A. Chaker, M. Sadok, M. Mostefaoui, and S. Lachtar, Modeling and Simulation of Photovoltaic Module and Array Based on One and Two Diode Model Using Matlab/Simulink, Energy Procedia **74**, 864 (2015).
3. T. Jin and J. Kim, A comparative study of energy and carbon efficiency for emerging countries using panel stochastic frontier analysis, Sci Rep **9**, 6647 (2019).
4. A. Barbón, V. Carreira-Fontao, L. Bayón, and C. A. Silva, Optimal design and cost analysis of single-axis tracking photovoltaic power plants, Renewable Energy **211**, 626 (2023).
5. H. M. Ridha, A. A. Heidari, M. Wang, and H. Chen, Boosted mutation-based Harris hawks optimizer for parameters identification of single-diode solar cell models, Energy Conversion and Management **209**, 112660 (2020).
6. F. F. Muhammadsharif, S. Hashim, S. S. Hameed, S. K. Ghoshal, I. K. Abdullah, J. E. Macdonald, and M. Y. Yahya, Brent's algorithm based new computational approach for accurate determination of single-diode model parameters to simulate solar cells and modules, Solar Energy **193**, 782 (2019).
7. A. Yahya-Khotbehsara and A. Shahhoseini, A fast modeling of the double-diode model for PV modules using combined analytical and numerical approach, Solar Energy **162**, 403 (2018).
8. E. Q. B. Macabebe, C. J. Sheppard, and E. E. van Dyk, Parameter extraction from I–V characteristics of PV devices, Solar Energy **85**, 12 (2011).
9. A. Askarzadeh and A. Rezazadeh, Artificial bee swarm optimization algorithm for parameters identification of solar cell models, Applied Energy **102**, 943 (2013).
10. A. Askarzadeh and L. dos Santos Coelho, Determination of photovoltaic modules parameters at different operating conditions using a novel bird mating optimizer approach, Energy Conversion and Management **89**, 608 (2015).
11. M. S. Ismail, M. Moghavvemi, and T. M. I. Mahlia, Characterization of PV panel and global optimization of its model parameters using genetic algorithm, Energy Conversion and Management **73**, 10 (2013).
12. K. M. El-Naggar, M. R. AlRashidi, M. F. AlHajri, and A. K. Al-Othman, Simulated Annealing algorithm for photovoltaic parameters identification, Solar Energy **86**, 266 (2012).
13. M. F. AlHajri, K. M. El-Naggar, M. R. AlRashidi, and A. K. Al-Othman, Optimal extraction of solar cell parameters using pattern search, Renewable Energy **44**, 238 (2012).
14. M. G. Villalva, J. R. Gazoli, and E. R. Filho, Modeling and circuit-based simulation of photovoltaic arrays, (2009).
15. J. Appelbaum and A. Peled, Parameters extraction of solar cells – A comparative examination of three methods, Solar Energy Materials and Solar Cells **122**, 164 (2014).
16. Y. Chahet, M. E. Amraoui, A. E. Amrani, A. Bouaichi, B. Aksasse, and L. Bejjit, Determination of Polycrystalline Photovoltaic Module Degradation Rate Based on Electrical Parameters Estimation, in Proceedings of the 4th International Conference on Innovative Research in Applied Science, Engineering and Technology, IRASET, 15-16 May, Fez, Morocco (2024)

17. T. Easwarakhanthan, J. Bottin, I. Bouhouch, and C. Boutrit, Nonlinear Minimization Algorithm for Determining the Solar Cell Parameters with Microcomputers, International Journal of Solar Energy (1986).
18. K. Yu, B. Qu, C. Yue, S. Ge, X. Chen, and J. Liang, A performance-guided JAYA algorithm for parameters identification of photovoltaic cell and module, Applied Energy **237**, 241 (2019).
19. N. Pourmousa, S. M. Ebrahimi, M. Malekzadeh, and M. Alizadeh, Parameter estimation of photovoltaic cells using improved Lozi map based chaotic optimization Algorithm, Solar Energy **180**, 180 (2019).
20. A. M. Beigi and A. Maroosi, Parameter identification for solar cells and module using a Hybrid Firefly and Pattern Search Algorithms, Solar Energy **171**, 435 (2018).